

<sup>9</sup>A. Fahlman, K. Hamrin, G. Axelson, C. Nordling, and K. Siegbahn, *Z. Physik* **192**, 484 (1966).

<sup>10</sup>J. Tauc, in *Progress in Semiconductors* (Temple, London, 1965), Vol. 9, p. 120.

PHYSICAL REVIEW B

VOLUME 3, NUMBER 8

15 APRIL 1971

## Frequency Upconversion in $\text{YF}_3 : \text{Yb}^{3+}, \text{Tm}^{3+}$

F. W. Ostermayer, Jr., J. P. van der Ziel, H. M. Marcos,  
L. G. Van Uitert, and J. E. Geusic

*Bell Telephone Laboratories, Murray Hill, New Jersey 07974*

(Received 5 October 1970)

The stepwise conversion of infrared ( $\approx 0.97 \mu$ ) radiation to near infrared ( $0.81 \mu$ ) and visible ( $0.475 \mu$ ) light in  $\text{YF}_3$  sensitized with  $\text{Yb}^{3+}$  and activated with  $\text{Tm}^{3+}$  has been studied in detail. The lifetimes and fluorescence intensities of the important manifolds ( $\text{Yb } ^2F_{5/2}$ ,  $\text{Tm } ^3H_4$ ,  $\text{Tm } ^3F_4$ , and  $\text{Tm } ^1G_4$ ), as well as the Yb-to-Tm transfer probability coefficients for the three steps of the process, have been measured as functions of concentration. A saturation effect previously observed in the Tm emission versus infrared excitation intensity has been shown to result from the rate of depopulation of  $\text{Tm } ^3H_4$  by the second Yb-to-Tm transfer exceeding the  $\text{Tm } ^3H_4$  decay rate. This was used to determine the second transfer probability coefficient. The first transfer probability coefficient was found to be  $1.2 \times 10^{-17} \text{ cm}^3 \text{ sec}^{-1}$  independent of Tm concentration and for Yb concentration of the order of 10 at. % and greater. The second transfer probability coefficient was found to be approximately  $10^{-14} \text{ cm}^3 \text{ sec}^{-1}$  for Yb concentrations of 25 at. % and greater. The third transfer probability coefficient was found to be  $2.7 \times 10^{-16} \text{ cm}^3 \text{ sec}^{-1}$ . The dependence on Yb concentration of the relative efficiency of conversion to  $0.475\text{-}\mu$  light agrees well with the values calculated from a rate-equation model using the measured lifetimes and transfer probability coefficients.

### I. INTRODUCTION

The conversion of infrared ( $\approx 0.97 \mu$ ) radiation to near infrared ( $0.81 \mu$ ) and visible ( $0.475 \mu$ ) light has been observed<sup>1-5</sup> in a number of host crystals sensitized with  $\text{Yb}^{3+}$  and activated with  $\text{Tm}^{3+}$ . Since the conversion process is particularly efficient in  $\text{YF}_3$ ,<sup>5</sup> a detailed study has been made to correlate the efficiency with the characteristics of Yb and Tm in this material. This paper presents the results of the study.

Section II discusses the model for the conversion process and pertinent results are derived from the rate equations. The assumptions implicit in the rate equations are also discussed. Section III deals with the fluorescence lifetime and intensity measurements of the important Yb and Tm levels and Sec. IV with the Yb-to-Tm transfer probabilities. In Sec. V, these results are used to calculate the conversion efficiency. Reasonable agreement with the experimental efficiency and with the variation of efficiency with Yb concentration is obtained.

### II. CONVERSION MECHANISM AND RATE EQUATIONS

The model for the conversion process which agrees with our observed results is that proposed by Auzel<sup>1</sup> involving stepwise excitation of Tm by nonresonant energy transfer from Yb and multiphonon decay in Tm. The mechanism is illustrated schematically on the Yb and Tm energy-level dia-

grams<sup>6</sup> in Fig. 1. To the right-hand side of each manifold is its spectroscopic label, and to the left-hand side is a label which is more conveniently used in the rate equations below. Step 1 is a nonresonant transfer in which  $1650 \text{ cm}^{-1}$  must be absorbed by the lattice,  $1'$  is a multiphonon decay, 2 is a nonresonant transfer with  $1000 \text{ cm}^{-1}$  absorbed by the lattice,  $2'$  are multiphonon decays, and 3 is a nonresonant transfer with  $1400 \text{ cm}^{-1}$  absorbed by the lattice. The  $0.81\text{-}\mu$  emission results from the  $\text{Tm } ^3F_4 \rightarrow ^3H_6$  transition and that at  $0.475 \mu$  from  $\text{Tm } ^1G_4 \rightarrow ^3H_6$ .

The steady-state rate equations appropriate to this model are

$$\frac{dn_{Y2}}{dt} = \frac{\sigma_Y I}{\epsilon_Y} n_{Y1} - \frac{n_{Y2}}{\tau_Y} - \chi_1 n_{Y2} n_{T1} - \chi_2 n_{Y2} n_{T2} - \chi_3 n_{Y2} n_{T4} = 0, \quad (1)$$

$$\frac{dn_{T2}}{dt} = \chi_1 n_{Y2} n_{T1} - \frac{n_{T2}}{\tau_{T2}} - \chi_2 n_{Y2} n_{T2} = 0, \quad (2)$$

$$\frac{dn_{T4}}{dt} = \chi_2 n_{Y2} n_{T2} - \frac{n_{T4}}{\tau_{T4}} - \chi_3 n_{Y2} n_{T4} = 0, \quad (3)$$

$$\frac{dn_{T7}}{dt} = \chi_3 n_{Y2} n_{T4} - \frac{n_{T7}}{\tau_{T7}} = 0, \quad (4)$$

where  $\sigma_Y$  is the  $\text{Yb } ^2F_{7/2} \rightarrow ^2F_{5/2}$  cross section averaged over the spectrum of the exciting radiation,  $\epsilon_Y$  is the average energy of the  $\text{Yb } ^2F_{7/2} \rightarrow ^2F_{5/2}$  transition,  $I$  is the total intensity of the exciting

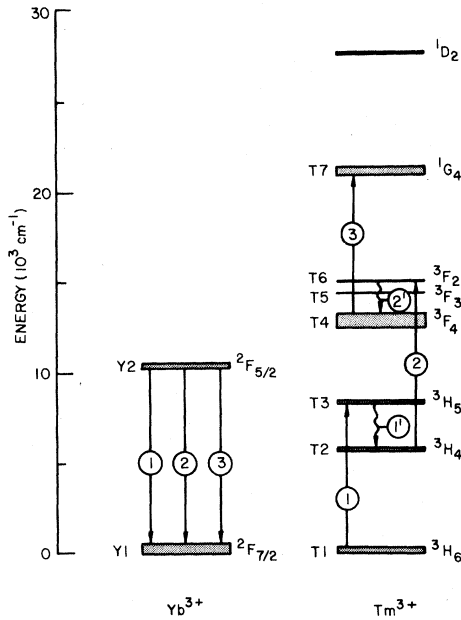


FIG. 1. Energy-level diagram of  $\text{Yb}^{3+}$  and  $\text{Tm}^{3+}$  showing the steps in the upconversion process.

radiation, the  $n$ 's are number densities of ions in the levels, the  $\tau$ 's are total lifetimes of the levels, and the  $\chi$ 's are the Yb-to-Tm transfer probability coefficients.

A number of approximations have been made in these equations. Back transfer from Tm to Yb has been neglected owing to the large energy differences between initial and final states in all transfers. Further, it has been assumed that the effect of the first and second Yb-to-Tm transfers is simply to populate T2 and T4, respectively, although the transfers are actually to T3 and T6 with subsequent multiphonon decay to T2 and T4. Therefore, there is the possibility of other routes of decay from these intermediate states and, in fact, some emission is seen from T3, T5, and T6 to the ground state. However, these emissions are much weaker than that from T2 and T4 and, hence, it is not unreasonable to neglect the effect of the intermediate states. The effects of transitions from T4 and T7 to lower-lying excited Tm states either by radiative or non-radiative (including quenching) processes have been neglected. They will be partially included by using the measured lifetimes which are concentration dependent. The above equations also neglect excitation from T7 to higher Tm states by transfer from Yb. Although some emission is observed from Tm  $^1D_2$ , it is much weaker than that from T7 at the excitation intensities used in these experiments. Finally, the form of these equations implies that the  $\chi$ 's are independent of concentrations and populations. In general this would not be expected to be true. The reason for its validity in our experi-

ments (as shown by our data) will be discussed in Sec. IV.

In obtaining solutions of these equations the approximation will be made that the Yb and Tm excited-state populations are small compared to the ground population so that  $n_{Y1} \approx n_Y$  and  $n_{T1} \approx n_T$ , where  $n_Y$  and  $n_T$  are the densities of Yb and Tm ions, respectively. This is valid at the excitation intensities used in our experiments.

Furthermore, the last term in Eqs. (1) and (3) will be neglected as it is only important when a saturation effect is observed in  $n_{T4}$ . At the excitation intensities we used, this is not the case.

With these approximations the total powers radiated per unit volume at 0.81 and 0.475  $\mu$  in terms of the excited Yb population  $n_{Y2}$  are

$$P(0.81 \mu) = \frac{\epsilon_{T41}}{\tau_{T41}^r} \frac{\tau_{T4} \chi_1 \chi_2 n_T n_{Y2}^2}{(\tau_{T2})^{-1} + \chi_2 n_{Y2}} \quad (5)$$

and

$$P(0.475 \mu) = \frac{\epsilon_{T71}}{\tau_{T71}^r} \tau_{T7} \tau_{T4} \frac{\chi_1 \chi_2 \chi_3 n_T n_{Y2}^3}{(\tau_{T2})^{-1} + \chi_2 n_{Y2}} \quad (6)$$

where  $\epsilon_{T41}$  and  $\epsilon_{T71}$  are the average photon energies, and  $\tau_{T41}^r$  and  $\tau_{T71}^r$  are the radiative lifetimes for the T4-T1 and T7-T1 transitions, respectively.

The relation between intensity and  $n_{Y2}$  can be obtained from Eqs. (1) (again neglecting the last term) and (2) and is

$$I = \frac{\epsilon_Y}{\sigma_Y n_Y} \left[ \frac{1}{\tau_Y} + \chi_1 n_T \left( 1 + \frac{1}{1 + (\tau_{T2} \chi_2 n_{Y2})^{-1}} \right) \right] n_{Y2} \quad (7)$$

Equation (7) together with Eqs. (5) and (6) describe the conversion per unit volume in terms of the excitation intensity and the material parameters. To determine the total power converted the physical arrangement of phosphor and exciting radiation must be known and an appropriate integration carried out. This will be discussed somewhat further in Sec. V.

### III. LIFETIME AND INTENSITY MEASUREMENTS

The  $\text{YF}_3$  phosphors were prepared by a  $\text{BeF}_2$  flux method described elsewhere<sup>7</sup> and were analyzed spectroscopically to verify the concentrations of the dopants.

The fluorescence lifetimes of the states appearing in the rate equations were measured by exciting a powdered sample with a short pulse of radiation from a GaAs:Si diode (Texas Instruments TIXL 12) or from a xenon flash lamp (EG&G FX-12-0.25) and observing the decay of the luminescence with a monochromator (Bausch and Lomb 33-86-25) and lead sulphide cell or RCA 7102 photomultiplier or EMI 9558 photomultiplier as appropriate. The exciting wavelengths were isolated from the flash lamp by means of Corning color glass and interfer-

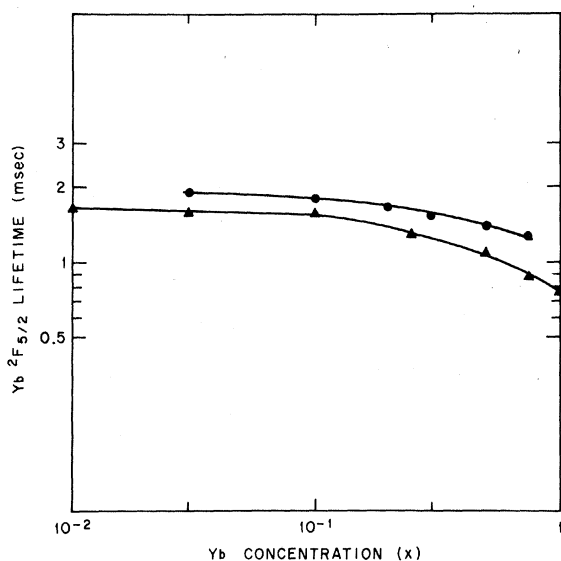


FIG. 2. Dependence of  $\text{Yb } ^2F_{5/2} 1/e$  lifetime on Yb concentration for the series  $\text{Y}_{1-x}\text{Yb}_x\text{F}_3$  (●) and  $\text{Y}_{0.9997-x}\text{Yb}_x\text{Tm}_{0.0003}\text{F}_3$  (▲).

ence filters. The excitation source and detection method for each level measured is shown in Table I.

The light pulse from the xenon lamp is approximately  $3 \mu\text{sec}$  wide at the half-intensity points which limits the shortest lifetimes that can be measured to a few  $\mu\text{sec}$ . The time constant of the PbS cell was 1.8 msec and, hence, was easily separated from the much longer  $\text{Tm } ^3H_4$  lifetime ( $\approx 13.5 \text{ msec}$ ).

The decays were in general nonexponential (as is expected when energy transfer and quenching effects are involved<sup>8</sup>) and have been characterized by a lifetime  $\tau_e$  which is the time for the intensity to fall to  $1/e$  of its initial value. It has been demonstrated<sup>9</sup> that this choice results in a concentration dependence which is very similar to that for the emission per ion or quantum yield. Hence,  $\tau_e$  is a lifetime which represents an average probability of decay of an excited ion and it is reasonable to use it in the rate equations.

The self-quenching of Yb and the  $^3F_4$  and  $^1G_4$

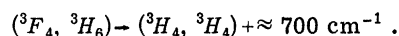
TABLE I. Excitation and detection methods used for lifetime measurements.

Level	Excitation source	Filters	Detector
$\text{Yb } ^2F_{5/2}$	GaAs : Si diode	•••	7102 PMT
$\text{Tm } ^3H_4$	GaAs : Si diode	•••	PbS cell
$\text{Tm } ^3F_4$	Xe lamp	0.706- $\mu$ interference	7102 PMT
$\text{Tm } ^1G_4$	Xe lamp	CS 5-57 + CS3-72	9558 PMT

manifolds of Tm was measured in the series  $\text{Y}_{1-x}\text{Yb}_x\text{F}_3$  and  $\text{Y}_{1-x}\text{Tm}_x\text{F}_3$  and is shown in Figs. 2 and 3, respectively. The quenching of  $\text{Tm } ^3H_4$ ,  $^3F_4$ , and  $^1G_4$  by Yb was measured in the series  $\text{Y}_{0.9997-x}\text{Yb}_x\text{Tm}_{0.0003}\text{F}_3$  and is shown in Fig. 4, while the quenching of Yb by Tm was measured in  $\text{Y}_{0.8-x}\text{Yb}_{0.2}\text{F}_3$  and is shown in Fig. 5.

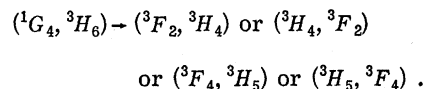
From Fig. 2, Yb exhibits a weak self-quenching which may be due to energy migration to defects (impurities, vacancies, etc., which can act as sinks for the Yb excitation energy) or to energy transfer to the ground-state manifolds of several neighboring Yb ions combined with phonon emission. The observed quenching of  $\text{Tm } ^3H_4$  by Yb favors the former mechanism as explained later.

The self-quenching of  $\text{Tm } ^3F_4$  (Fig. 3) results from the nonresonant ion-pair relaxation process



The  $700 \text{ cm}^{-1}$  was estimated from the Tm energy-level diagram.<sup>6</sup> As the maximum phonon energy in  $\text{YF}_3$  is approximately  $530 \text{ cm}^{-1}$ ,<sup>9</sup> the above is a two-phonon process.

The self-quenching of  $\text{Tm } ^1G_4$  (Fig. 3) is only slightly stronger than that for  $\text{Tm } ^3F_4$ . It is expected to be stronger since it results from the four resonant ion-pair relaxation processes



The quenching of  $\text{Tm } ^3H_4$  by Yb (Fig. 4) is extremely slight and may result from energy transfer to the ground-state manifolds of several neighboring Yb ions combined with phonon emission. This is a more likely process here than in the self-quenching of Yb, since the  $\text{Tm } ^3H_4 \rightarrow ^3H_6$  energy is less than

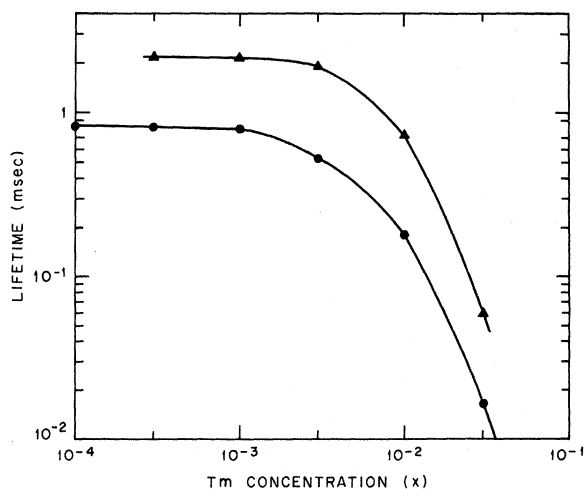


FIG. 3. Dependence of  $\text{Tm } ^3F_4$  (▲) and  $\text{Tm } ^1G_4$  (●)  $1/e$  lifetimes on Tm concentration in the series  $\text{Y}_{1-x}\text{Tm}_x\text{F}_3$ .

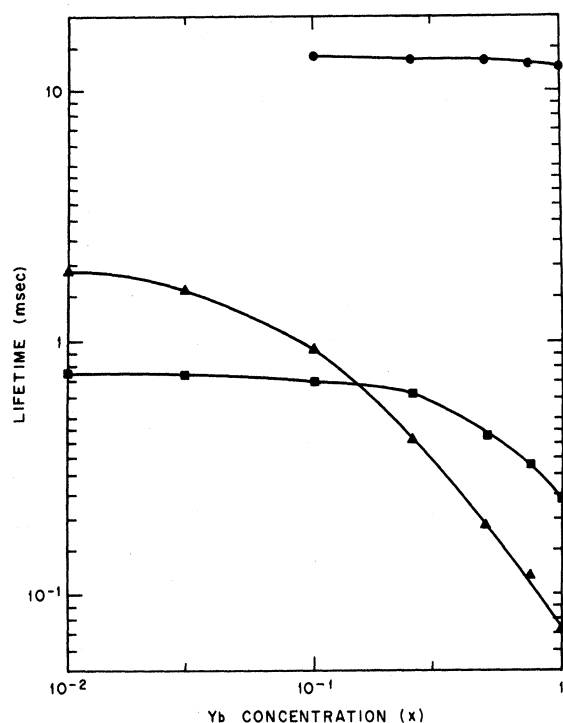
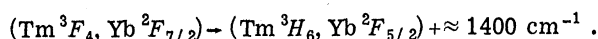


FIG. 4. Dependence of  $Tm^3H_4$  (●),  $Tm^3F_4$  (▲), and  $Tm^1G_4$  (■)  $1/e$  lifetimes on Yb concentration in the series  $Y_{0.9997-x}Yb_xTm_{0.0003}F_3$ .

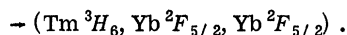
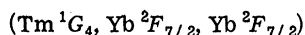
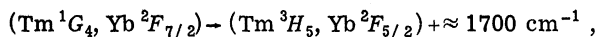
that for  $Yb^2F_{5/2} \rightarrow ^2F_{7/2}$ . The  $Tm^3H_4$  quenching is even weaker than the Yb self-quenching, which is strong evidence in favor of the migration to defects mechanism for the Yb self-quenching.

The quenching of  $Tm^3F_4$  by Yb (Fig. 4) is due to the nonresonant transfer process



The  $1400 \text{ cm}^{-1}$  was estimated from the  $Tm^3F_4$  emission and  $Yb^2F_{7/2}$  absorption spectra and corresponds to the emission of three phonons in  $YF_3$ .

Two mechanisms can contribute to the quenching of  $Tm^1G_4$  by Yb (Fig. 4),

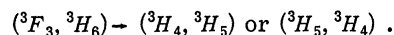


The first, a nonresonant ion-pair relaxation process, requires the emission of four phonons, and therefore, should be less probable than the three phonon quenching process for  $Tm^3F_4$ . The second requires the interaction with two Yb ions and, hence, does not become effective until a higher Yb concentration than for an ion-pair process. This explains the observed quenching of  $Tm^1G_4$  by Yb compared with that of  $Tm^3F_4$ .

The effects of nonradiative decay and energy transfer on the emission from the  $Tm^3F_4$  and  $^1G_4$

manifolds are shown in Figs. 6 and 7, respectively. The phosphors were excited with the Bausch and Lomb monochromator equipped with a tungsten light source and the resulting emission was detected by a photomultiplier after filtering with a second monochromator.

The emission per Tm ion (obtained by dividing the data for the series  $Y_{1-x}Tm_xF_3$  by the Tm concentration) from the  $^1G_4$  manifold has the same concentration dependence as the  $Tm^1G_4$  lifetime data in Fig. 3. The emission per Tm ion from the  $^3F_4$  manifold decreases more rapidly with concentration than the corresponding lifetime in Fig. 3. The difference is due to strong quenching of the  $^3F_3$  manifold by the resonant ion-pair relaxation processes



The  $^3F_4$  manifold is excited via the  $^3F_{2,3}$  manifolds; hence when the decay rate of  $^3F_3$  by the above quenching processes becomes comparable to the multiphonon decay rate to  $^3F_4$ , the emission from  $^3F_4$  also reflects the quenching of  $^3F_3$ . For the series  $Y_{1-x}Yb_{x-0.0003}Tm_{0.0003}F_3$ , the concentration dependence of the emission is directly comparable with the dependence of the lifetimes of Fig. 4.

These results show that, relative to the self-quenching of Tm, Yb is less effective in quenching the Tm emission. This is of significance for obtaining efficient upconversion. As is the case for usual luminescence, the concentration of active ions for upconversion is optimized when the luminescence is concentration independent. This occurs when the slope of the concentration-dependent quenching curve counterbalances the slope of the intrinsic concentration dependences of Eqs. (5) and (6).

From Figs. 6 and 7, the optimum Tm concentration, obtained from the peak of the Tm emission curve, is  $\approx 0.003$ . Assuming saturation of the  $^3H_4$  level, the optimum Yb concentration for  $^3F_4$  emission occurs when the quenching rate becomes linearly dependent on concentration, or at  $\approx 0.3$ . For

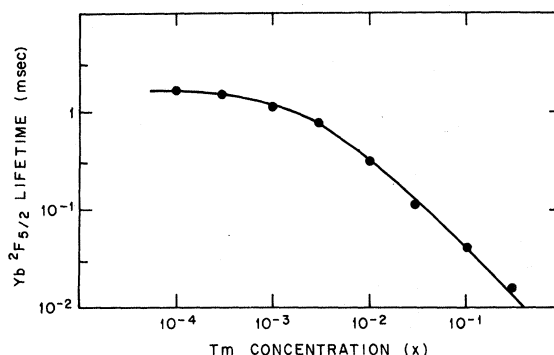


FIG. 5. Dependence of  $Yb^2F_{5/2}$   $1/e$  lifetime on Tm concentration in the series  $Y_{0.9-x}Yb_{0.2}Tm_xF_3$ .

$^1G_4$  emission, the optimum concentration is  $\approx 0.35$ . These results are in good agreement with the experimental values. Furthermore, we shall show in Sec. V that good agreement between theory and experiment is found over a wide range of Yb concentrations.

#### IV. TRANSFER PROBABILITIES

The first transfer probability coefficient  $\chi_1$  can be determined from the dependence of the Yb  $^2F_{5/2}$  lifetime on Tm concentration shown in Fig. 5 for the series  $Y_{0.8-x}Yb_{0.2}Tm_xF_3$ . From this data we can also determine whether  $\chi_1$  is independent of Tm concentration.

Under pulsed excitation (short compared to the total lifetime of Yb  $^2F_{5/2}$ ) the decay of the Yb  $^2F_{5/2}$  population, based on Eq. (1), is described by

$$\frac{dn_{Y2}}{dt} = -\frac{n_{Y2}}{\tau_Y} - \chi_1 n_{Y2} n_T. \quad (8)$$

Terms in Eq. (1) which are higher order in  $n_{Y2}$  have been neglected in Eq. (8). Equation (8) predicts an exponential decay with a lifetime

$$\tau = (1/\tau_Y + \chi_1 n_T)^{-1}. \quad (9)$$

Figure 5 shows the Yb  $^2F_{5/2}$  lifetime as a function of Tm concentration in the series  $Y_{0.8-x}Yb_{0.2}Tm_xF_3$ . The experimental points have been fitted by Eq. (9) with  $\tau_Y = 1.65$  msec and  $\chi_1 = 1.2 \times 10^{-17}$  cm<sup>3</sup> sec<sup>-1</sup>. The good agreement indicates that  $\chi_1$  is independent of Tm concentration for this series. For the series  $Y_{0.9-x}Yb_{0.1}Tm_xF_3$ , the Yb  $^2F_{5/2}$  lifetime could also be fitted by Eq. (9) with the same value of  $\chi_1$ . For the series  $Y_{0.999-x}Yb_{0.001}Tm_xF_3$ , however, Eq. (9) did not fit the experimental Yb  $^2F_{5/2}$  lifetimes. This implies that energy migration among the Yb ions is responsible for the indepen-

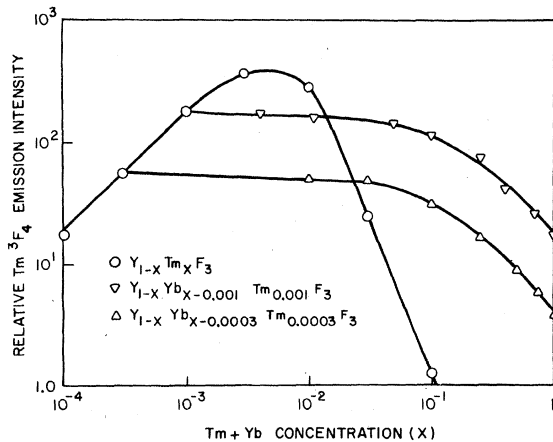


FIG. 6. Total Tm  $^3F_4$  to  $^3H_6$  emission as a function of the combined Tm and Yb concentration when the Tm  $^3F_{2,3}$  manifolds are excited.

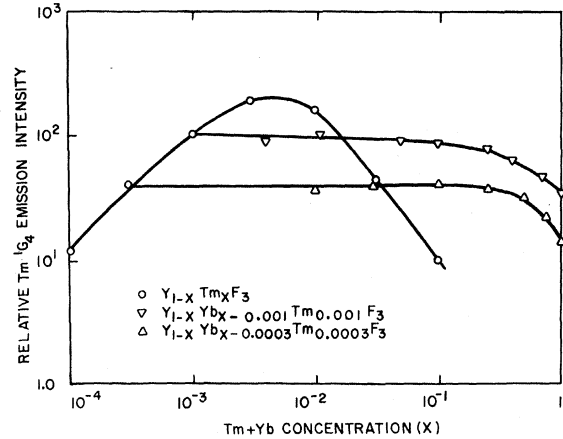


FIG. 7. Total Tm  $^1G_4$  to  $^3H_4$  emission as a function of the combined Tm and Yb concentration when the Tm  $^1G_4$  manifold is directly excited.

dence of  $\chi_1$  on Tm concentration.<sup>10</sup>

The second transfer probability coefficient  $\chi_2$  was determined from a saturation effect which occurs in the intensity of the Tm emission versus 0.93- $\mu$  excitation intensity. This effect was attributed by Hewes and Sarver<sup>3</sup> to depletion of the Tm ground state. Ground-state depletion, however, is ruled out from the values of the Tm  $^3H_4$ ,  $^3F_4$ , and  $^1G_4$  lifetimes, and the Yb absorption cross section. For ground-state depletion, the rate of emission from Tm excited states is too large by well over an order of magnitude to be accounted for by the rate of excitation of Yb at the intensities used in these experiments.

The effect is in fact due to the saturation of the Tm  $^3H_4$  population which occurs when the rate of depletion by the second transfer exceeds the natural decay rate  $1/\tau_{T2}$ . From the equation

$$n_{T2} = \chi_1 n_{Y2} n_T / [(\tau_{T2})^{-1} + \chi_2 n_{Y2}] \quad (10)$$

obtained from Eq. (2) together with Eq. (7), it is seen that the saturation behavior depends on  $\chi_2$ . Actually, if the multiphonon decay from  $T_4$  to  $T_2$  (via  $T_3$ ) were included in the rate equations,  $\chi_2$  in Eq. (10) would be replaced by  $(1 - A_{42}\tau_{T4})\chi_2$ , where  $A_{42}$  is the multiphonon decay rate from  $T_4$  to  $T_2$ . That is, the effective transfer rate would be reduced by the rate at which ions are excited to  $T_4$  by transfer decay back to  $T_2$ . The contribution of  $A_{42}$  to  $\tau_{T4}$  was not determined experimentally but an estimate based on the work of Weber<sup>11</sup> and of Riseberg and Moos<sup>12</sup> and the YF<sub>3</sub> phonon spectrum<sup>9</sup> gives  $A_{42}\tau_{T4} \approx \frac{1}{7}$ . Therefore, the multiphonon decay from  $T_4$  causes a minor error in the determination of  $\chi_2$ .

Figure 8 shows the variation of the Tm  $^3H_4$  (1.84  $\mu$ ) intensity with 0.93- $\mu$  excitation intensity for several members of the series  $Y_{0.9997-x}Yb_xTm_{0.0003}F_3$ . The data was taken by painting a very thin layer of

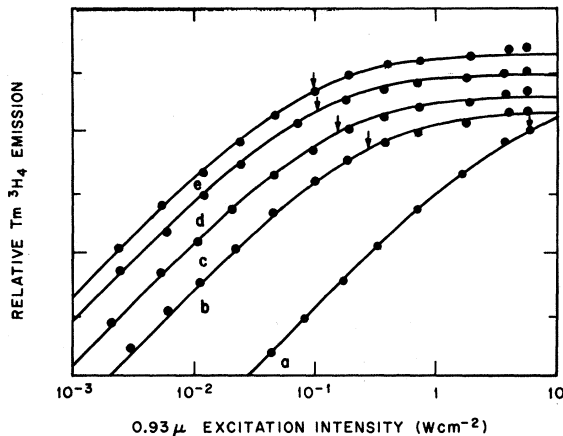


FIG. 8. Saturation of  $\text{Tm}^3H_4$  emission as a function of  $0.93\text{-}\mu$  excitation intensity from a GaAs:Si diode for  $x=0.1$ —curve a;  $x=0.25$ —b;  $x=0.5$ —c;  $x=0.75$ —d, and  $x=0.9997$ —e in the series  $\text{Y}_{0.9997-x}\text{Yb}_x\text{Tm}_{0.0003}\text{F}_3$ .

a phosphor-glycerine mixture onto the dome of a GaAs:Si diode to insure uniform excitation intensity within the phosphor. The diode was driven with a 17-Hz current square wave which is sufficiently slow so that the phosphor emission intensity depended on the peak output of the diode. The  $1.84\text{-}\mu$  emission was isolated with a germanium window and Bausch and Lomb 33-86-25 monochromator and detected with a lead sulphide cell and lock-in amplifier. At the low diode current levels the diode output was monitored with a RCA 7102 PM tube with filters to select the wavelength and attenuate the radiation for operation in the linear region of the PM tube. At the high levels, the diode current was used to determine the diode output by a separate measurement of output power versus diode current using an elliptical reflector to collect the diode radiation and a thermopile to measure the power. This allowed the total power output of the diode to be determined for each data point. An average intensity was obtained by dividing by the surface area of the dome.

The data in Fig. 8 have been fitted by Eq. (10) with  $n_{Y_2}$  assumed to be proportional to the intensity  $I$ . This is not strictly true as Eq. (7) varies from

$$I = \frac{\epsilon_Y}{\sigma_Y n_Y} \left( \frac{1}{\tau_Y} + \chi_1 n_T \right) n_{Y_2}$$

at low intensities, to

$$I = \frac{\epsilon_Y}{\sigma_Y n_Y} \left( \frac{1}{\tau_Y} + 2\chi_1 n_T \right) n_{Y_2}$$

at high intensities. The departure from proportionality is small, however, as  $1/\tau_Y \approx 10^3 \text{ sec}^{-1}$  and  $\chi_1 n_T = 76 \text{ sec}^{-1}$ . In determining the value of  $\chi_2$  the average relation

$$I = \frac{\epsilon_Y}{\sigma_Y n_Y} \left( \frac{1}{\tau_Y} + 1.5\chi_1 n_T \right) n_{Y_2}, \quad (11)$$

which is the relation when  $1/\tau_{T_2} = \chi_2 n_{Y_2}$ , was used. The value of  $\sigma_Y$  is  $9.1 \times 10^{-22} \text{ cm}^2$ . This was determined by graphical integration of the product of the absolute absorption spectrum of a small crystallite of  $\text{Y}_{0.82}\text{Yb}_{0.18}\text{F}_3$  (measured on a Cary 14 with reducing optics) and the emission spectrum of the GaAs:Si diode. The quantity  $1/\tau_Y + 1.5\chi_1 n_T$  was obtained from the Yb lifetime for the series  $\text{Y}_{0.9997-x}\text{Yb}_x\text{Tm}_{0.0003}\text{F}_3$  shown in Fig. 2 and the value of  $\chi_1$  obtained previously.

The values of  $\chi_2$  calculated from this data for the different Yb concentrations are shown in Table II. For the 25% and greater Yb concentration  $\chi_2$  is relatively constant. The 10% Yb sample, however, shows an appreciably lower value. This may appear inconsistent with the result that  $\chi_1$  is the same for 10% and 20% Yb concentrations. A possible explanation for this inconsistency is the larger value of  $\chi_2$ . The independence of the transfer probability coefficients on Yb and Tm concentrations is due to the energy migration in the Yb being rapid compared to the rate of transfer. Therefore, the faster the transfer, the more rapid the migration for this condition to hold and the higher the Yb concentration at which it does.

The dependence of  $\chi_2$  on Tm concentration could not be measured due to the strong self-quenching of the  $\text{Tm}^3F_4$  manifold (Fig. 3) which rapidly repopulates the  $\text{Tm}^3H_4$  manifold and reduces the effective transfer rate. Hence, it is clear that the effective transfer coefficient will be a strong function of Tm concentration due to this effect and it would be very difficult to separate out any intrinsic dependence of  $\chi_2$  on Tm concentration.

The third transfer probability coefficient  $\chi_3$  was determined from the ratio of the efficiencies of conversion to  $0.81\text{-}$  and  $0.475\text{-}\mu$  radiation in the material  $\text{Y}_{0.649}\text{Yb}_{0.35}\text{Tm}_{0.001}\text{F}_3$ . The measurements were made in a calibrated integrating sphere and the ratio of the powers at an excitation intensity of  $\approx 4 \text{ W cm}^{-2}$  was  $P(0.475 \mu)/P(0.81 \mu) = 3.6 \times 10^{-2}$ . Using Eqs. (5) and (6) to determine the power ratio in terms of  $\chi_3$ , the value obtained is  $\chi_3 = 2.7 \times 10^{-16} \text{ cm}^3 \text{ sec}^{-1}$ .

TABLE II. Values of  $\chi_2$  determined from saturation data in Fig. 6 for  $\text{Y}_{0.9997-x}\text{Yb}_x\text{Tm}_{0.0003}\text{F}_3$ .

Yb concentration ( $x$ )	$\chi_2$ ( $\text{cm}^3 \text{ sec}^{-1}$ )
0.10	$9.9 \times 10^{-16}$
0.25	$8.8 \times 10^{-15}$
0.50	$10.1 \times 10^{-15}$
0.75	$11.6 \times 10^{-15}$
0.9997	$10.9 \times 10^{-15}$

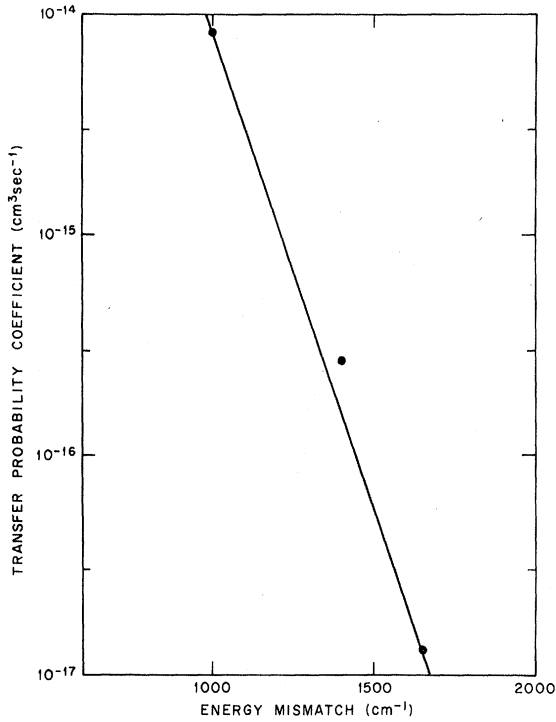


FIG. 9. Semilogarithmic plot of the transfer probability coefficients for the three Yb-to-Tm transfers as a function of the energy mismatch between initial and final electronic states.

Since  $\chi_1$ ,  $\chi_2$ , and  $\chi_3$  represent transfers with different degrees of nonresonance, it is interesting to compare their magnitudes against the energy mismatch for each. As in the case of multiphonon decay within a single ion<sup>12</sup> it would be expected on the basis of perturbation theory that  $\chi \propto \bar{W}^{\bar{n}}$ , where  $\bar{W}$  is an average probability for the emission of a phonon in the transfer process and  $\bar{n}$  is an average number of phonons which must be emitted. Since  $\bar{n} \propto \Delta E$ , the energy mismatch,  $\log_{10}\chi$  would be expected to be a linear function of  $\Delta E$ .  $\log_{10}\chi_1$ ,  $\log_{10}\chi_2$ , and  $\log_{10}\chi_3$  have been plotted versus  $\Delta E$  in Fig. 9 and it is interesting to note that the three points do lie in approximately a straight line.

#### V. DEPENDENCE OF CONVERSION EFFICIENCY ON Yb CONCENTRATION

Using the lifetimes and transfer probability coefficients determined in Sec. III and IV, we have calculated the variation of the conversion efficiency with Yb concentration from the equations in Sec. II. The comparison of this calculation with the measured variation serves as a check on the model as reflected in the rate equations.

To measure the relative efficiency the radiation from a GaAs:Si diode was focused with an elliptical reflector onto the surface of a powdered sample in

an optical cell and the 0.475- $\mu$  luminescence was monitored with a "spectra" brightness spot meter (Photo Research Corp.). This method was used to determine the relative efficiency as a function of Yb concentration in the series  $Y_{0.9997-x}Yb_xTm_{0.0003}F_3$ .

In this method, the 0.93- $\mu$  intensity was too low for the saturation of Tm  $^3H_4$  to occur. Therefore, in comparing the calculated and measured relative efficiencies, the effect of the saturation denominator in Eq. (6) can be neglected.

Equation (6), combined with Eq. (7), gives the 0.475- $\mu$  power density generated at a point at which the excitation intensity is  $I$ . In order to obtain the total power generated, an integration appropriate to the physical configuration of source and phosphor must be performed. It is not possible to treat the powdered phosphor exactly so we resort to a model which contains the essential features.<sup>13</sup> This is to consider the powder to be equivalent to a uniform layer of material of thickness  $d$ . Neglecting saturation, the Yb concentration dependence of the total 0.475- $\mu$  power generated is

$$P_T(0.475 \mu) \propto \frac{\tau_T \tau_T \tau_T \tau_T \tau_T}{[(\tau_Y)^{-1} + \chi_1 n_T]^3} \chi_2 x^2 (1 - e^{-\sigma_Y n x d}), \quad (12)$$

where  $n$  is the number density of cation sites ( $2.10 \times 10^{22} \text{ cm}^{-3}$  for  $YF_3$ ),  $x$  is the fractional Yb concentration, and it has been assumed that  $\chi_3$  is independent of Yb concentration.

Two limiting cases can be distinguished in Eq. (12). If the effective thickness is such that  $\sigma_Y n x d \ll 1$  (optically thin), then the explicit concentration dependence is  $x^3$ . If  $\sigma_Y n x d \gg 1$  (optically thick), then the explicit dependence is  $x^2$ . The best agreement between theory and experiment is obtained with the assumption that the phosphor is optically thick for the Yb concentrations used.

The relative efficiency versus Yb concentration was calculated using the Tm lifetimes in Fig. 4, the Yb lifetimes in Fig. 2 for the series  $Y_{0.9997-x}Yb_xTm_{0.0003}F_3$ , and the values of  $\chi_2$  in Table II. The resulting curve is shown in Fig. 10 together with the experimental points. The calculated curve was normalized to fit the experimental point at  $x = 0.25$ . The agreement is good for the points at  $x = 0.5$ , 0.75, and 0.9997. There is, however, some discrepancy for  $x = 0.1$ . There are several sources of error which might account for the difference. The experimental error in the value of  $\chi_2$  for  $x = 0.1$  is probably larger than that for the other concentrations since only a slight degree of saturation could be attained in this material. Nonetheless, the agreement between calculation and experiment in Fig. 10 confirms the model and the approximations made in the rate equations.<sup>14</sup>

#### VI. SUMMARY AND CONCLUSIONS

From this work, a quantitative understanding of

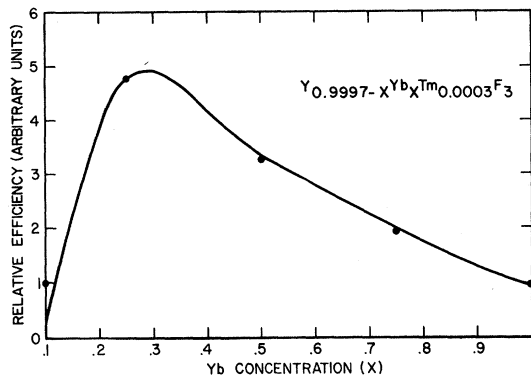


FIG. 10. Comparison between measured and calculated relative efficiency of conversion of  $0.93\text{-}\mu$  radiation to  $0.475\text{-}\mu$  light as a function of Yb concentration.

the frequency upconversion process in  $\text{YF}_3$ , sensitized with Yb and activated with Tm, has been obtained. The parameters (lifetimes, intensities, and transfer probability coefficients) which determine the efficiency of the conversion process were measured and used to calculate efficiencies from a simple rate-equation model. The correlation between the measured and calculated efficiencies is good.

A saturation effect in the dependence of Tm emis-

sion on infrared excitation intensity has been explained and was used as the basis for determining the transfer probability coefficient for the second Yb-to-Tm transfer.

The energy difference between the initial and final electronic states is different for each of the three transfers involved in the conversion process and we have compared the transfer probabilities with the energy mismatches using the model in which the probability depends on the average number of phonons emitted in the transfer. The three experimental points support this model.

The main limitation on the efficiency of the conversion to  $0.475\text{-}\mu$  light is the quenching of the  $\text{Tm}^3F_4$  and  $^1G_4$  manifolds by Yb as seen in Fig. 4 from the lifetimes and in Figs. 6 and 7 from the intensity data. This is a fundamental limitation in the sense that the quenching results from the same interaction between Yb and Tm ions which is responsible for the excitation of the Tm ions in the first place. Therefore, the increase in efficiency which would result from larger Yb-to-Tm transfer probabilities would be at least partially offset by the enhanced quenching of the  $\text{Tm}^3F_4$  and  $^1G_4$  manifolds.

#### ACKNOWLEDGMENTS

We wish to thank P. H. Buhite and W. H. Grodkiewicz for technical assistance.

<sup>1</sup>F. Auzel, *Compt. Rend.* **263B**, 819 (1966).

<sup>2</sup>V. V. Ovsyankin and P. P. Feofilov, *Zh. Eksperim. i Teor. Fiz. Pis'ma v Redaktsiyu* **4**, 471 (1966) [*Soviet Phys. JETP Letters* **4**, 317 (1966)].

<sup>3</sup>R. A. Hewes and J. F. Sarver, *Phys. Rev.* **182**, 427 (1969).

<sup>4</sup>R. A. Hewes, *J. Luminescence* **1**, 778 (1970).

<sup>5</sup>J. E. Geusic, F. W. Ostermayer, H. M. Marcos, J. P. van der Ziel, and L. G. Van Uitert, *J. Appl. Phys.* **42**, 1958 (1971).

<sup>6</sup>Taken from the energy-level diagram in G. H. Dieke, *Spectra and Energy Levels of Rare Earth Ions in Crystals* (Interscience, New York, 1968), p. 142.

<sup>7</sup>L. G. Van Uitert, L. Pictroski, and W. H. Grodkiewicz, *Mater. Res. Bull.* **4**, 777 (1969).

<sup>8</sup>See, for example, L. G. Van Uitert, E. F. Dearborn, and J. J. Rubin, *J. Chem. Phys.* **47**, 3653 (1967).

<sup>9</sup>H. E. Rast, H. H. Caspers, and S. A. Miller, *Phys. Rev.* **180**, 890 (1969).

<sup>10</sup>The same effect of migration has been observed by

L. G. Van Uitert, E. F. Dearborn, and J. J. Rubin [*J. Chem. Phys.* **45**, 1578 (1966)] in the quenching of  $\text{Tb}^{3+}$  by  $\text{Sm}^{3+}$  and by L. G. Van Uitert, E. F. Dearborn, and H. M. Marcos [*Appl. Phys. Letters* **9**, 255 (1966)] in the quenching of  $\text{Tb}^{3+}$  by  $\text{Eu}^{3+}$ .

<sup>11</sup>M. J. Weber, *Phys. Rev.* **171**, 283 (1968).

<sup>12</sup>L. A. Riseberg and H. W. Moos, *Phys. Rev.* **174**, 429 (1968).

<sup>13</sup>J. P. van der Ziel, F. W. Ostermayer, and L. G. Van Uitert, *Phys. Rev. B* **2**, 4432 (1970).

<sup>14</sup>Absolute conversion efficiencies were measured with a calibrated integrating sphere for a slurry of phosphor and glycerine applied directly to a diode dome. This is described in Ref. 5. The result was a conversion efficiency of about 0.1% for the  $0.475\text{-}\mu$  emission. It is difficult to make an accurate calculation for this configuration but an estimate based on a plane wave incident on a semi-infinite crystal gives approximately the measured value.